Predominant myosin super-relaxed state in canine myocardium with naturally occurring dilated cardiomyopathy

Julien Ochala[1]*, Christopher T. A. Lewis[1], Thomas Beck[1], Hiroyuki Iwamoto[2], Sarah Kosta[3], Kenneth S. Campbell[3,4], W. Glen Pyle[5,6]

1. Department of Biomedical Sciences, University of Copenhagen, Copenhagen, Denmark
2. SPring-8, Japan Synchrotron Radiation Research Institute, Hyogo, Japan
3. Department of Physiology, University of Kentucky, Lexington, Kentucky, USA
4. Division of Cardiovascular Medicine, University of Kentucky, Lexington, Kentucky, USA
5. IMPART Investigator Team, Dalhousie Medicine, Saint John, New Brunswick, Canada
6. Department of Biomedical Sciences, University of Guelph, Guelph, Ontario, Canada

*Corresponding author: julien.ochala@sund.ku.dk

Highlights

- The proportion of cardiac myosin heads in the super-relaxed state is greater in left ventricles of Doberman Pinschers with dilated cardiomyopathy than in non-failing dogs.
- The length dependent activation of myosin heads is prevented disrupting force generation.
- A small molecule known to activate myosin (EMD-57033) partially counterbalances the super-relaxed state disturbance.

Abstract

Dilated cardiomyopathy (DCM) is a naturally occurring heart failure condition in humans and dogs, notably characterized by a reduced ejection fraction. As the identification of the underlying cellular and molecular mechanisms remain incomplete, the aim of the present study was to assess whether myosin and its known relaxed conformational states contribute to DCM aetiology. For that, we dissected and skinned thin cardiac strips from left ventricle obtained from six DCM Doberman Pinschers and six nonfailing controls (NF). We then used Mant-ATP chase experiments, X-ray diffraction and molecular simulations. We observed that, in DCM dogs, the amount of myosin heads in the stabilizing conformational state also known as super-relaxed (SRX) is significantly increased when compared with NF dogs. We also found that myosin heads are blocked in this SRX state preventing a proper length dependent activation, subsequently hindering myosin head recruitment and force-generating capacity. Despite these, our data also demonstrate that when applying EMD-57033, a small molecule activating myosin, SRX-related detrimental effects can be rescued. Taken together, our results suggest that myosin SRX contributes to the DCM pathophysiology and that the observed negative changes are reversible, giving hope for a myosin-centered pharmacological treatment of this particular cardiac disease.

Key words: Heart; Dilated Cardiomyopathy; Doberman Pinschers; Myosin

1. Introduction

Dilated cardiomyopathy (DCM) is a naturally occurring disease in humans and dogs with several large breed dogs including Doberman Pinschers, Great Danes and Newfoundlands being at a high risk. In the case of Doberman Pinschers, up to 60% of dogs are diagnosed with DCM [1, 2]. The age of onset of such disease varies but dogs usually experience cardiac dilatation and a dramatically reduced contractile function of the left or both ventricles, as attested by the diminished ejection fraction and cardiac output. These ultimately lead to ventricular wall thinning, myocardial fibrosis, congestive heart failure, and a rapid and devastating decline in the quality of life [3]. Recent discoveries point to a multi-gene basis potentially involving the *PDK4* and *TTN* genes, respectively encoding for pyruvate dehydrogenase kinase 4 and titin [4, 5]. Hence, veterinary medicine has seen tremendous progress in the genetics of Doberman DCM, and yet it remains a fatal condition whose pathophysiological causes are unclear [3, 6, 7]. Indeed, the precise cascade of negative cellular and molecular events triggering the diminished contractile function still needs exploring.

In healthy hearts, stroke volume increases with the preload that fills the heart during diastole. This phenomenon called the Frank-Starling Law relies on the proper functioning of sarcomeric proteins, myosin head positioning, and their length-dependent activation (LDA) [8, 9]. In diastole, the two myosin heads can either (i) interact with each other and with the filament backbone or (ii) be mobile. In the first case known as the super-relaxed state (SRX), the heads are sequestered, restricted from interacting with actin monomers, and have a very low ATPase rate. In the second conformation called the disordered-relaxed state (DRX), myosin heads are free to bind to actin filaments and have a ten-fold higher ATPase activity [10, 11]. Preload defined as the filling of ventricles, stretches cardiac cells, increases sarcomere length (SL), and thought to promote a myosin head shift from SRX to DRX states, allowing a fast transition to actin binding when thin filaments are switched on by Ca^{2+} ions [9]. The increased DRX:SRX ratio at longer SL is then suggested to enhance myofibril Ca^{2+} sensitivity and maximum force-generating capacity during systole [9].

Interestingly, in Doberman Pinschers, the sensitivity to Ca^{2+} ions as well as the maximum force production of cardiac myofibrils is dramatically impaired [12]. Hence, in the present study, we initailly hypothesised that dogs with naturally occurring DCM would exhibit a pathological higher proportion of cardiac myosin molecules blocked in the SRX conformation that would then be insensitive to SL change. This would have negative consequences for the number of myosin heads available to bind to actin

monomers and for the subsequent cellular force generation, contributing to the DCM phenotype. To test our hypothesis, we used both nonfailing controls (NF) and naturally occurring DCM dog left ventricle samples. We then isolated thin cardiac strips and applied the Mant-ATP chase protocol at short and long SL, together with X-ray diffraction and molecular simulations.

2. Results

To test our initial hypothesis, we started by evaluating the proportions and ATP turnover times of DRX and SRX myosin heads in cardiac strips isolated from NF and DCM dogs. For that, we used a loaded Mant-ATP chase protocol consisting of recording the rate of ATP consumption of resting skinned cardiac bundles (Fig. 1A) [13]. A total of 428 individual cardiac strips were tested (8 to 10 cardiac bundles for each of the twelve dogs, at each of the two SLs and with or without EMD-57033).

2.1. Higher proportion of myosin molecules in the SRX conformation in DCM dogs

At short SL (2.00 µm), DCM dogs displayed slower Mant-ATP consumptions as attested by the significantly lower DRX to SRX ratio when compared with NF dogs (Fig. 1B). Despite this, the DRX and SRX ATP turnover lifetimes were unchanged (Fig. 1C-D). To get structural insights into the lower DRX to SRX ratio, we recorded X-ray diffraction patterns from a subset of isolated cardiac thin bundles from NF and DCM dogs. This allowed us to analyze high-quality myosin meridional reflections, also known as M3 and M6 [9]. To further ensure reliable and interpretable data, all the recorded images were summed up for each condition (NF versus DCM dogs). We observed that, M3, indicative of the distance/order between myosin heads, and M6, representative of myosin filament backbone periodicity, had unchanged spacings. Nevertheless, the M3 intensity was greater in DCM dogs when compared with NF dogs whilst M6 intensity was unaffected (Fig. 2A-B). These indicate a higher magnitude of myosin head order in DCM dogs. These observations are consistent with the lower DRX to SRX ratio that we found using the Mant-ATP chase protocol.

To better understand whether these functional and structural findings would have consequences on myosin recruitment, we ran molecular simulations. We applied a computational tool, FiberSim 2.1.0 (https://campbell-muscle-lab.github.io/FiberSim/), which is a spatially explicit myofilament model that is able to mimic the force generation [14]. When implementing an increase of the proportion of SRX myosin molecules by 10%, to decrease the DRX to SRX ratio by approximately a third (as it happens in DCM dogs when compared with NF animals), simulations showed a small decrease in isometric force (at maximal and sub-maximal activation levels) and a rightward shift of the Force-pCa curve leading to a lower Ca^{2+} sensitivity (Fig. 3A-B). These imply that when the DRX to SRX ratio is lowered in DCM dogs, myosin head recruitment for force production may subtlety be impaired.

2.2. Stretch-insensitive myosin molecules and diminished LDA in DCM dogs

At long SL (2.30 µm), NF dogs exhibited a leftward shift in the double exponential decay curve of Mant-ATP consumption (Fig. 1A). Indeed, in this group of dogs, upon stretching of the cardiac strips, the DRX to SRX ratio was increased (Fig. 1B) whilst the DRX ATP turnover time was decreased significantly (Fig. 1C), supporting the concept of myosin head LDA (Fig. 1E-G) [9]. On the other hand, in DCM dogs, myosin molecules were insensitive to stretch; DRX to SRX ratio as well as DRX and SRX ATP turnover times were unaffected (Fig. 1B-D). Hence, the myosin head LDA was non-existent (Fig. 1E-G).

2.3. Partially restored amounts of myosin heads in the SRX heads in DCM dogs with EMD-57033

To test the reversibility of the disrupted DRX to SRX ratio in DCM dogs, we used a commercially available pharmacological compound, EMD-57033 (EMD). EMD is a thiadiazinone derivative that is known to bind to an allosteric pocket in the myosin motor domain [15] and promote myosin DRX state [16]. In the presence of 10 µM of EMD, NF and DCM dogs had faster Mant-ATP consumptions. At short SL, the DRX to SRX ratio was significantly increased for both NF and DCM dogs (Fig. 1B). However, DRX and SRX ATP turnover lifetimes were unchanged (Fig. 1C-D). At long SL, with the addition of 10 µM of EMD, in NF dogs, the DRX to SRX ratio was not enhanced (Fig. 1B) while the DRX ATP turnover time was significantly shorter (Fig. 1C). In DCM dogs, even though EMD had beneficial effects, the DRX to SRX ratio as well as DRX and SRX ATP turnover lifetimes were not altered by the stretch (Fig. 1B-D). Our findings then suggest that, in the presence of EMD, the stretch activation of myosin heads is abolished in all dogs; EMD and LDA are then likely to share some common mechanisms (Fig. 1E-G).

3. Discussion

Here, in line with our initial hypothesis, we demonstrate that DCM dogs have a diminished DRX to SRX ratio at short and long SLs when compared with NF dogs, impairing the LDA, myosin head recruitment, and force production. We also show that the changes are reversible by using a pharmacological compound acting as a myosin activator, EMD.

3.1. Impaired DRX to SRX ratio as a pathological determinant in DCM

At short SL, our finding of disrupted DRX to SRX ratio is novel in the context of canine DCM but has previously been linked to the disease aetiology of human hypertrophic cardiomyopathy (HCM) due to *MYH7* or *MYPBC3* mutations (encoding for β/slow myosin heavy chain or for myosin-binding protein C, respectively) [17, 18]. For instance, the *MYH7*-associated mutations cause single amino acid substitutions in the myosin head-head interface or head-tail region. These weaken the formation of the interacting heads motif crucial for myosin head sequestration and for the SRX state [19]. Hence, in HCM, the greater DRX to SRX ratio induces an enhanced availability of myosin heads for actin binding, fitting well with the long-lasting hyper-contractility hypothesis [18, 19]. Because *MYH7* or *MYPBC3* sequences are highly conserved across species, the impact of the mutations is believed to be the same among a wide range of mammal species including dogs. Human *MYH7* mutations linked to DCM appear to have totally opposite effects [19]. Indeed, the variants stabilize the interacting heads motif and subsequent SRX conformation reducing the number of myosin heads available for recruitment. Fewer heads can enter the force-generating phase leading to hypo-contractility and having detrimental consequences for the pumping action of the heart [19, 20].

In contrast to *MYH7*-associated HCM or DCM, in the present study, the observed reduced DRX to SRX ratio cannot be caused by the direct molecular effect of the mutations on the interacting heads motif but rather to other unexplored processes. Cardiac myosin molecules have a very slow turnover rate of 1-2% per day [21], they can face and be regulated by multiple post-translational modifications [22]. Previously, it has been shown that DCM dogs have decreased phosphorylation levels of the myosin regulatory light chain (RLC) when compared with NF dogs [12]. Cardiac RLC phosphorylation is thought to regulate myosin SRX state [23] with its de-phosphorylation stabilizing the ordered array of myosin heads bound to the thick filament backbone [24]. Thus, we speculate that, in DCM dogs, the RLC de-phosphorylation alters myosin head positioning and promotes myosin head sequestration. Further studies specifically verifying this hypothesis are warranted.

3.2. Blunted LDA of relaxed myosin heads in DCM

In addition to observing an altered disrupted myosin DRX to SRX ratio at short SL, we, demonstrate here for the first time that, when SL is increased, the usual shift from SRX to DRX states is abolished in DCM dogs. The exact underlying mechanisms of this blockade remain unclear but may also be related to the RLC de-phosphorylation reported previously in DCM dogs when compared with NF dogs [12]. In the normal diastole, stretching cardiac cells (preload) is thought to allow the recruitment of myosin heads from the reserve SRX pool, improving the systole [9]. Here, in DCM dogs, this recruitment is blunted, preventing fast binding to actin monomers and compromising subsequent maximum force-generating capacity. This disturbance may represent an under-appreciated component of the DCM phenotype that may be drug targetable.

3.3. Potential beneficial effects of EMD-57033 on SRX myosin molecules

As Doberman Pinscher DCM is highly likely caused by multi-gene mutations [4, 5], gene therapy may not be feasible in the near future, necessitating an alternate approach in which the functional basis of the cardiac disease is targeted instead. Towards this end, small molecules directly interfering with myosin have emerged in the context of human heart failure offering great promise for veterinary medicine [25]. Activating myosin pharmacologically would avoid the disadvantages of classic inotropic agents that improve cardiac contractility but also increase oxygen demand and heart rate, and are linked to hypotension, arrhythmia, and increased mortality [26]. Besides Omecamtiv Mecarbil and Danicamtiv, EMD has been proven to be both a Ca^{2+}-sensitizer acting on cardiac troponin and a direct myosin activator [15]. Very few studies have investigated its potency in DCM. In the present study, we found a partial restoration of the DRX to SRX ratio in the presence of EMD, indicating that with treatment the myosin heads move away from the filament backbone toward the actin monomers, promoting cross-bridge formation and increasing the overall Ca^{2+}-sensitivity of force production. Even though EMD has a low bio-availability and has never been tested in clinical trials [16], our results provide evidence that other related small molecules activating myosin with similar characteristics may be potent and relevant for treating DCM.

4. Conclusions

Our findings indicate that, in isolated cardiac strips from DCM dogs, the myosin-stabilizing conformational state also known as SRX is favoured when compared with cardiac bundles from NF dogs.

Our data also suggest that such remodelling is likely to negatively impact LDA as well as subsequent myosin head recruitment and force-generating capacity, providing a potential molecular mechanism for the disease. Nevertheless, these alterations can be rescued by applying myosin activators such as EMD. Taken together, all our results give new important insights into the under-appreciated canine DCM pathophysiology and further strengthen the potential benefits of drugs targeting myosin activity in dogs, and also potentially in humans.

5. Methods

5.1. Dog left ventricular collection

Animals were cared for in accordance with the guidelines of the Animal Care and Use Committee of the University of Guelph and the Canadian Council on Animal Care [12]. Table 1 summarises NF and DCM dogs' characteristics. Tissue samples were obtained from the left ventricle free wall of Doberman Pinschers with advanced DCM causing congestive heart failure (whose owners were electing humane death) or dogs with no previous history of cardiovascular disease (NF). Written consent was obtained from clients for all procedures, including for the collection of myocardial samples [12]. Samples were rapidly frozen in liquid nitrogen and stored at −80°C for the measurements explained below.

5.2. Solutions

As previously published [27, 28], the relaxing solution contained 4 mM Mg-ATP, 1 mM free Mg^{2+}, $10^{-6.00}$ mM free Ca^{2+}, 20 mM imidazole, 7 mM EGTA, 14.5 mM creatine phosphate and KCl to adjust the ionic strength to 180 mM and pH to 7.0. Additionally, the rigor buffer for Mant-ATP chase experiments contained 120 mM K acetate, 5 mM Mg acetate, 2.5 mM K_2HPO_4, 50 mM MOPS, 2 mM DTT with a pH of 6.8. For experiments involving EMD-57033, all experimental solutions contained 10 µM EMD-57033 (gift from Dr Norbert Beier, E. Merck Pharmaceuticals).

5.3. Muscle preparation and fibre permeabilisation

Cryopreserved left ventricle samples were dissected into thin bundles and immersed in a membrane-permeabilising solution (relaxing solution containing glycerol; 50:50 v/v) for 24 hours at -20°C, after which they were transferred to 4°C. These bundles were kept in the membrane-permeabilising solution at 4°C for an additional 24 hours (to allow a proper skinning/membrane permeabilisation process). After these steps, bundles were stored in the same buffer at -20°C for use up to one week [29, 30].

5.4. Mant-ATP chase experiments

On the day of the experiments, bundles were transferred to the relaxing solution and thin cardiac strips (approximately 50 µm wide) were isolated. Their ends were individually clamped to half-split copper meshes designed for electron microscopy (SPI G100 2010C-XA, width, 3 mm), which had been glued to glass slides (Academy, 26 x 76 mm, thickness 1.00-1.20 mm). Cover slips were then attached to the top (using double-sided tape) to create flow chambers (Menzel-Gläser, 22 x 22 mm, thickness 0.13-0.16 mm) [27, 28]. Subsequently, at 25°C, for each cardiac strip, the SL was either set at 2.00 or 2.30 µm using the

brightfield mode of a Zeiss Axio Scope A1 microscope. Similar to previous studies [27, 28], each thin strip was first incubated for five minutes with a rigor buffer. A solution containing the rigor buffer with 250 µM Mant-ATP was then flushed and kept in the chamber for five minutes. At the end of this step, another solution made of the rigor buffer with 4 mM ATP was added with simultaneous acquisition of the Mant-ATP chase.

For fluorescence acquisition, a Zeiss Axio Scope A1 microscope was used with a Plan-Apochromat 20x/0.8 objective and a Zeiss AxioCam ICm 1 camera. Frames were acquired every five seconds with a 20 ms acquisition/exposure time using a DAPI filter set, for five minutes. Three regions of each individual myofibre were sampled for fluorescence decay using the ROI manager in ImageJ as previously published [27, 28]. The mean background fluorescence intensity was subtracted from the average of the fibre fluorescence intensity (for each image taken). Each time point was then normalized by the fluorescence intensity of the final Mant-ATP image before washout (T = 0). These data were then fit to an unconstrained double exponential decay using Graphpad Prism 9.0:

$$\text{Normalised Fluorescence} = 1 - P1\,(1-\exp^{(-t/T1)}) - P2\,(1-\exp^{(-t/T2)})$$

Where P1 (DRX) is the amplitude of the initial rapid decay approximating the disordered-relaxed state with T1 as the time constant for this decay. P2 (SRX) is the slower second decay approximating the proportion of myosin heads in the super-relaxed state with its associated time constant T2 [27].

5.5. X-ray diffraction recordings and analyses

On the day of the experiments, thin cardiac strips were placed in a plastic dish containing the relaxing solution. They were then transferred to the specimen chamber, filled with the relaxing buffer. The ends of these thin muscle bundles were then clamped at a SL of 2.00 µm. Subsequently, X-ray diffraction patterns were recorded at 15°C using a CMOS camera (Model C11440-22CU, Hamamatsu Photonics, Japan, 2048 x 2048 pixels) in combination with a 4-inch image intensifier (Model V7739PMOD, Hamamatsu Photonics, Japan). The exposure time was 500 ms or 1 s. The X-ray wavelength was 0.10 nm and the specimen-to-detector distance was 2.14 m. For each preparation, approximately 20-30 diffraction patterns were recorded at the BL40XU beamline of SPring-8 and were analysed as described previously [31]. To minimize radiation damage, the exposure time was kept low (2 s) and the specimen chamber was moved by 100 µm after each exposure. Following X-ray recordings, background scattering was subtracted,

and the major myosin meridional reflection intensities/spacing were determined as described elsewhere previously [31, 32].

5.6. Molecular Simulations

The FiberSim 2.1.0 software has been thoroughly described previously [14]. Briefly, FiberSim tracks the position and status of actin and myosin molecules within a network of compliant thick and thin filaments. For all the simulations, the half-sarcomere lattice was composed of 100 thick filaments and 200 thin filaments. These filaments were arranged in a hexagonal lattice to mimic the architecture of mammalian muscle. Filaments located at the edge of the lattice were "mirrored" on the opposite side to minimize edge effects [33]. Each thin filament was composed of two actin strands. Each strand contained 27 regulatory units, and each regulatory unit contained 7 binding sites. Each thick filament was composed of 54 myosin crowns with each crown consisting of 3 pairs of myosin dimers. Each binding site on actin could be in an inactive (unavailable for myosin binding) or active (available for myosin binding) state. All seven binding sites from a regulatory unit switched simultaneously between those two states, depending on the Ca^{2+} concentration and on the transition rate constants k_{on} and k_{off} which we set. A cooperative mechanism was also implemented such that the transition probability for a regulatory unit was influenced by the states of its neighbours. Finally, a regulatory unit was prevented from deactivating if one or more myosin head(s) were bound.

Although this model only has two explicit thin filament states, it mimics an important feature of the three state thin filament model described by McKillop and Geeves [34] in that bound myosin heads inhibited relaxation. Heads in SRX switched to DRX at a rate k_1 that is assumed to be force-dependent [14]. DRX heads could then attach to available binding sites on actin. The attachment and detachment rates depended on x, where x is the distance to the binding site measured parallel to the filaments. The detachment rate function (k_4) was updated for the present study so that it had an exponential strain-dependence similar to that measured for single myosin heads via optical trapping [35]. Model parameters were chosen to reproduce physiological values for: maximal isometric force (≈ 150-200 kPa at a sarcomere length of 2.00 µm), passive force (≈ 1-2% of the maximal isometric force) and Ca^{2+} sensitivity ($pCa_{50} \approx 5.7$).

5.7. Statistical analysis

Echocardiographic data was analyzed using a one-way ANOVA. Comparison between groups of data was performed using a two-way ANOVA (with the following two factors: NF/DCM and EMD-57033+/-). All data are expressed as means ± standard deviations; graphs were prepared and analyzed in Graphpad Prism v9. Statistical significance was set to $p < 0.05$.

Funding: This work was generously funded by the Carlsberg Foundation (CF20-0113) grant to J.O. OVC Pet Trust funded the collection of canine samples (W.G.P.)

Acknowledgement: The X-ray experiments were performed under approval of the SPring-8 Proposal Review Committee (2022A1069). EMD-57033 was a gift from Dr. Norbert Beier from Merck KGaA, Darmstadt, Germany.

Conflicts of Interest: The authors report no conflicts of interest.

Author Contributions: JO, KSC and WGP conceived the study; JO and WGP acquired funding; JO, KSC and WGP managed the project; JO, CTAL, TB, HI, SK, KSC and WGP performed experiments; JO, CTAL, TB, HI, SK, KSC and WGP analyzed data and interpreted the results; JO, CTAL, TB, HI, SK, KSC and WGP wrote and reviewed the manuscript.

References

[1] M.J. Hazlett, M.G. Maxie, D.G. Allen, B.P. Wilcock, A retrospective study of heart disease in doberman pinscher dogs, Can Vet J 24(7) (1983) 205-10.
[2] G. Wess, A. Schulze, V. Butz, J. Simak, M. Killich, L.J. Keller, J. Maeurer, K. Hartmann, Prevalence of dilated cardiomyopathy in Doberman Pinschers in various age groups, J Vet Intern Med 24(3) (2010) 533-8.
[3] M.R. O'Grady, S.L. Minors, M.L. O'Sullivan, R. Horne, Effect of pimobendan on case fatality rate in Doberman Pinschers with congestive heart failure caused by dilated cardiomyopathy, J Vet Intern Med 22(4) (2008) 897-904.
[4] K.M. Meurs, J.A. Stern, D. Adin, B.W. Keene, T.C. De Francesco, S.P. Tou, Assessment of PDK4 and TTN gene variants in 48 Doberman Pinschers with dilated cardiomyopathy, J Am Vet Med Assoc 257(10) (2020) 1041-1044.
[5] S. Simpson, J. Edwards, R.D. Emes, M.A. Cobb, N.P. Mongan, C.S. Rutland, A predictive model for canine dilated cardiomyopathy-a meta-analysis of Doberman Pinscher data, PeerJ 3 (2015) e842.
[6] N.J. Summerfield, A. Boswood, M.R. O'Grady, S.G. Gordon, J. Dukes-McEwan, M.A. Oyama, S. Smith, M. Patteson, A.T. French, G.J. Culshaw, L. Braz-Ruivo, A. Estrada, M.L. O'Sullivan, J. Loureiro, R. Willis, P. Watson, Efficacy of pimobendan in the prevention of congestive heart failure or sudden death in Doberman Pinschers with preclinical dilated cardiomyopathy (the PROTECT Study), J Vet Intern Med 26(6) (2012) 1337-49.
[7] M.L. O'Sullivan, M.R. O'Grady, W.G. Pyle, J.F. Dawson, Evaluation of 10 genes encoding cardiac proteins in Doberman Pinschers with dilated cardiomyopathy, Am J Vet Res 72(7) (2011) 932-9.
[8] P.P. de Tombe, R.D. Mateja, K. Tachampa, Y. Ait Mou, G.P. Farman, T.C. Irving, Myofilament length dependent activation, J Mol Cell Cardiol 48(5) (2010) 851-8.
[9] W. Ma, M. Henze, R.L. Anderson, H. Gong, F.L. Wong, C.L. Del Rio, T. Irving, The Super-Relaxed State and Length Dependent Activation in Porcine Myocardium, Circ Res 129(6) (2021) 617-630.
[10] J.W. McNamara, A. Li, C.G. Dos Remedios, R. Cooke, The role of super-relaxed myosin in skeletal and cardiac muscle, Biophys Rev 7(1) (2015) 5-14.
[11] C.T.A. Lewis, J. Ochala, Myosin Heavy Chain as a Novel Key Modulator of Striated Muscle Resting State, Physiology (Bethesda) 38(1) (2023) 0.
[12] Y. Cheng, K.A. Hogarth, M.L. O'Sullivan, M. Regnier, W.G. Pyle, 2-Deoxyadenosine triphosphate restores the contractile function of cardiac myofibril from adult dogs with naturally occurring dilated cardiomyopathy, Am J Physiol Heart Circ Physiol 310(1) (2016) H80-91.
[13] P. Hooijman, M.A. Stewart, R. Cooke, A new state of cardiac myosin with very slow ATP turnover: a potential cardioprotective mechanism in the heart, Biophys J 100(8) (2011) 1969-76.
[14] S. Kosta, D. Colli, Q. Ye, K.S. Campbell, FiberSim: A flexible open-source model of myofilament-level contraction, Biophys J 121(2) (2022) 175-182.
[15] M.B. Radke, M.H. Taft, B. Stapel, D. Hilfiker-Kleiner, M. Preller, D.J. Manstein, Small molecule-mediated refolding and activation of myosin motor function, Elife 3 (2014) e01603.
[16] V. Jani, W. Qian, S. Yuan, T. Irving, W. Ma, EMD-57033 Augments the Contractility in Porcine Myocardium by Promoting the Activation of Myosin in Thick Filaments, Int J Mol Sci 23(23) (2022).
[17] C.N. Toepfer, A.C. Garfinkel, G. Venturini, H. Wakimoto, G. Repetti, L. Alamo, A. Sharma, R. Agarwal, J.F. Ewoldt, P. Cloonan, J. Letendre, M. Lun, I. Olivotto, S. Colan, E. Ashley, D. Jacoby, M. Michels, C.S. Redwood, H.C. Watkins, S.M. Day, J.F. Staples, R. Padron, A. Chopra, C.Y. Ho, C.S. Chen, A.C. Pereira, J.G. Seidman, C.E. Seidman, Myosin Sequestration Regulates Sarcomere Function, Cardiomyocyte Energetics, and Metabolism, Informing the Pathogenesis of Hypertrophic Cardiomyopathy, Circulation 141(10) (2020) 828-842.

[18] C.N. Toepfer, H. Wakimoto, A.C. Garfinkel, B. McDonough, D. Liao, J. Jiang, A.C. Tai, J.M. Gorham, I.G. Lunde, M. Lun, T.L.t. Lynch, J.W. McNamara, S. Sadayappan, C.S. Redwood, H.C. Watkins, J.G. Seidman, C.E. Seidman, Hypertrophic cardiomyopathy mutations in MYBPC3 dysregulate myosin, Sci Transl Med 11(476) (2019).
[19] L. Alamo, J.S. Ware, A. Pinto, R.E. Gillilan, J.G. Seidman, C.E. Seidman, R. Padron, Effects of myosin variants on interacting-heads motif explain distinct hypertrophic and dilated cardiomyopathy phenotypes, Elife 6 (2017).
[20] D.V. Rasicci, P. Tiwari, S.M.L. Bodt, R. Desetty, F.R. Sadler, S. Sivaramakrishnan, R. Craig, C.M. Yengo, Dilated cardiomyopathy mutation E525K in human beta-cardiac myosin stabilizes the interacting-heads motif and super-relaxed state of myosin, Elife 11 (2022).
[21] K. Smith, M.J. Rennie, The measurement of tissue protein turnover, Baillieres Clin Endocrinol Metab 10(4) (1996) 469-95.
[22] V. Vanhooren, A. Navarrete Santos, K. Voutetakis, I. Petropoulos, C. Libert, A. Simm, E.S. Gonos, B. Friguet, Protein modification and maintenance systems as biomarkers of ageing, Mech Ageing Dev 151 (2015) 71-84.
[23] T. Kampourakis, M. Irving, Phosphorylation of myosin regulatory light chain controls myosin head conformation in cardiac muscle, J Mol Cell Cardiol 85 (2015) 199-206.
[24] S.B. Scruggs, A.C. Hinken, A. Thawornkaiwong, J. Robbins, L.A. Walker, P.P. de Tombe, D.L. Geenen, P.M. Buttrick, R.J. Solaro, Ablation of ventricular myosin regulatory light chain phosphorylation in mice causes cardiac dysfunction in situ and affects neighboring myofilament protein phosphorylation, J Biol Chem 284(8) (2009) 5097-106.
[25] S.J. Lehman, C. Crocini, L.A. Leinwand, Targeting the sarcomere in inherited cardiomyopathies, Nat Rev Cardiol 19(6) (2022) 353-363.
[26] K. Alsulami, S. Marston, Small Molecules acting on Myofilaments as Treatments for Heart and Skeletal Muscle Diseases, Int J Mol Sci 21(24) (2020).
[27] J. Ochala, C.J. Finno, S.J. Valberg, Myofibre Hyper-Contractility in Horses Expressing the Myosin Heavy Chain Myopathy Mutation, MYH1(E321G), Cells 10(12) (2021).
[28] N. Ranu, J. Laitila, H.F. Dugdale, J. Mariano, J.S. Kolb, C. Wallgren-Pettersson, N. Witting, J. Vissing, J.J. Vilchez, C. Fiorillo, E. Zanoteli, M. Auranen, M. Jokela, G. Tasca, K.G. Claeys, N.C. Voermans, J. Palmio, S. Huovinen, M. Moggio, T.N. Beck, A. Kontrogianni-Konstantopoulos, H. Granzier, J. Ochala, NEB mutations disrupt the super-relaxed state of myosin and remodel the muscle metabolic proteome in nemaline myopathy, Acta Neuropathol Commun 10(1) (2022) 185.
[29] J.A. Ross, Y. Levy, M. Ripolone, J.S. Kolb, M. Turmaine, M. Holt, J. Lindqvist, K.G. Claeys, J. Weis, M. Monforte, G. Tasca, M. Moggio, N. Figeac, P.S. Zammit, H. Jungbluth, C. Fiorillo, J. Vissing, N. Witting, H. Granzier, E. Zanoteli, E.C. Hardeman, C. Wallgren-Pettersson, J. Ochala, Impairments in contractility and cytoskeletal organisation cause nuclear defects in nemaline myopathy, Acta Neuropathol 138(3) (2019) 477-495.
[30] J.A. Ross, H. Tasfaout, Y. Levy, J. Morgan, B.S. Cowling, J. Laporte, E. Zanoteli, N.B. Romero, D.A. Lowe, H. Jungbluth, M.W. Lawlor, D.L. Mack, J. Ochala, rAAV-related therapy fully rescues myonuclear and myofilament function in X-linked myotubular myopathy, Acta Neuropathol Commun 8(1) (2020) 167.
[31] J. Ochala, H. Iwamoto, L. Larsson, N. Yagi, A myopathy-linked tropomyosin mutation severely alters thin filament conformational changes during activation, Proc Natl Acad Sci U S A 107(21) (2010) 9807-12.
[32] M. Li, H. Ogilvie, J. Ochala, K. Artemenko, H. Iwamoto, N. Yagi, J. Bergquist, L. Larsson, Aberrant post-translational modifications compromise human myosin motor function in old age, Aging Cell 14(2) (2015) 228-35.
[33] B.C. Tanner, T.L. Daniel, M. Regnier, Sarcomere lattice geometry influences cooperative myosin binding in muscle, PLoS Comput Biol 3(7) (2007) e115.

[34] D.F. McKillop, M.A. Geeves, Regulation of the interaction between actin and myosin subfragment 1: evidence for three states of the thin filament, Biophys J 65(2) (1993) 693-701.
[35] C. Veigel, J.E. Molloy, S. Schmitz, J. Kendrick-Jones, Load-dependent kinetics of force production by smooth muscle myosin measured with optical tweezers, Nat Cell Biol 5(11) (2003) 980-6.

Tables

Table 1. Echocardiographic measurements from Doberman Pinschers. DCM, dilated cardiomyopathy; HR, heart rate; LVIDd, left ventricle internal diameter, end diastole; LVIDs, left ventricle internal diameter, end systole; FS, fractional shortening. Non-failing group consists of 2 female and 4 male dogs. DCM group is comprised of 3 male and 3 female dogs. Data are presented as mean ± standard deviation. * denotes a significant difference when compared with NF ($p < 0.05$).

	HR (bpm)	LVIDd (mm)	LVIDs (mm)	FS (%)
NF	98 ± 16	38.7 ± 0.6	27.3 ± 0.8	29.5 ± 1.7
DCM	172 ± 25*	61.3 ± 7.4*	52.0 ± 6.6*	15.1 ± 3.0*

Figures

Figure 1. Mant-ATP data. (A) Typical Mant-ATP chase experimental data show exponential decays for thin cardiac strips isolated from NF and DCM dogs at two SLs (short: 2.00 µm and long: 2.30 µm). (B) The resultant DRX to SRX ratio as well as (C) DRX ATP turnover time (T1) and (D) SRX ATP turnover time (T2) are displayed. Percent change with stretch (vs short SL) of DRX to SRX ratio (E), DRX ATP turnover time (F) and SRX ATP turnover time (G). Dots are dog's average data (out of 8 to 10 cardiac strips per dog). Means and standard deviations also appear on the graphs. * denotes a significant difference when compared with NF at the same SL ($p < 0.05$). # denotes a significant difference when compared with short SL for the same group ($p < 0.05$). & denotes a significant difference when compared with the same group at the same SL without 10 µM of EMD-57033 (EMD) ($p < 0.05$).

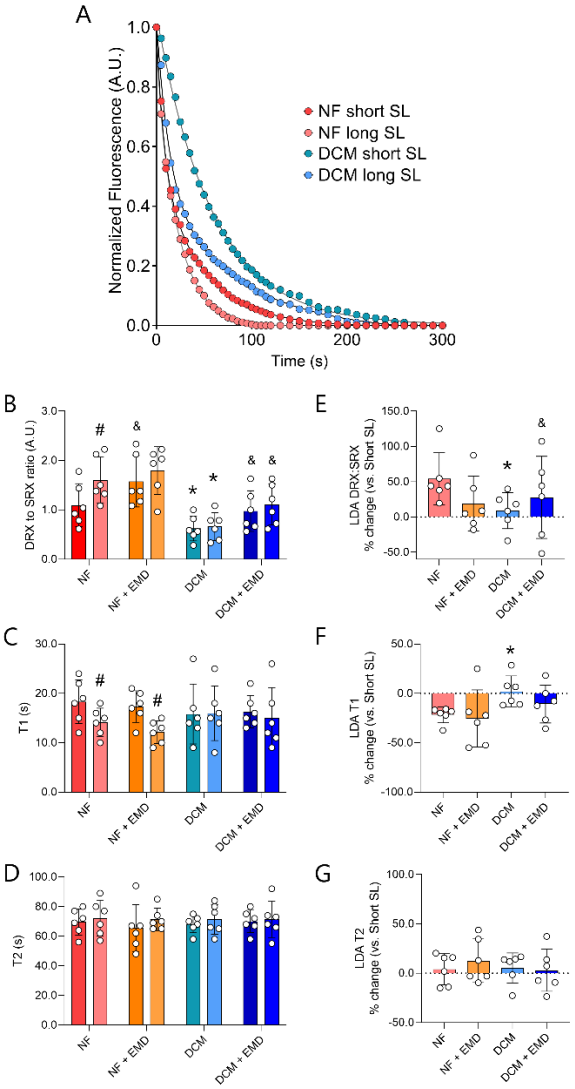

Figure 2. X-ray diffraction data. (A) Typical X-ray diffraction patterns obtained for thin cardiac strips isolated from NF and DCM dogs at a SL of 2.00 µm. (B) The table summarises M3 and M6 intensities normalised to the 6th actin-layer line and spacings.

A

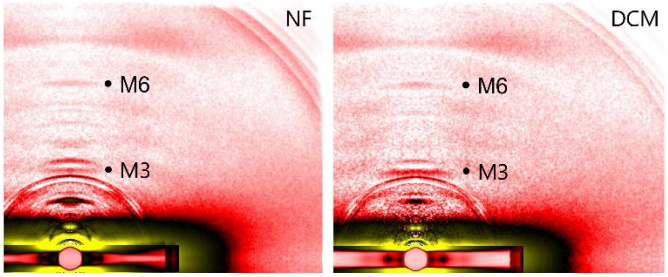

B

Group	M3		M6	
	Intensity	Spacing	Intensity	Spacing
NF	0.100	14.431	0.034	7.254
DCM	0.144	14.492	0.033	7.249

Figure 3. Molecular simulations. (A) shows the three-component model used for our simulation [14] with SRX, DRX and FG (force-generating) states. Here we tested an increase of the proportion of SRX myosin molecules by 10%, so a decrease of the DRX to SRX ratio by approximately a third. (B) and (C) are the results of the simulations in terms of force generating capacity at carious Ca^{2+} concentrations (Ca^{2+} sensitivity: pCa_{50} and Hill coefficient: n_H).

A

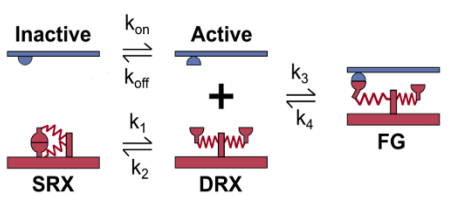

B

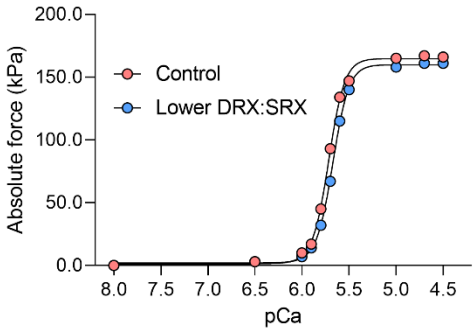

C

Group	pCa_{50}	n_H
NF	5.70	5.16
DCM	5.65	5.26